agronomy

MDPI

Article

Expression Pattern, Molecular Docking and Dynamics Simulation Analysis of CSP4 from *Sirex nitobei* Provides Molecular Basis of CSP Bound to Scent Molecules

Pingping Guo [1,†], Enhua Hao [1,†], Han Li [1], Xi Yang [1], Pengfei Lu [1,*] and Haili Qiao [2,*]

[1] The Key Laboratory for Silviculture and Conservation of the Ministry of Education, School of Forestry, Beijing Forestry University, Beijing 100083, China
[2] Institute of Medicinal Plant Development, Chinese Academy of Medical Sciences and Peking Union Medical College, Beijing 100193, China
* Correspondence: lpengfei224@126.com (P.L.); hlqiao@implad.ac.cn (H.Q.); Tel.: +86-10-6233-6755 (P.L.); +86-10-5783-3180 (H.Q.)
† These authors contributed equally to this work.

Abstract: Insects stimulate specific behaviors by correctly recognizing scent molecules in the external environment. *Sirex nitobei*, a wood-boring wasp species native to Asia with a distribution area that includes the Palaearctic and Oriental regions, is a significant pest of conifers. Focusing on the molecular mechanism of protein-ligand binding, this study resolved the tissue expression profile of CSP4 from *S. nitobei* (SnitCSP4) and probed its binding properties with target ligands using molecular docking and dynamics simulations to verify the odor recognition function of this protein. The open reading frame (ORF) of SnitCSP4 was 396 bp, encoding 131 amino acids. Tissue expression analysis revealed that *SnitCSP4* was significantly expressed in female antennae and docking showed that all ligands were bound in hydrophobic cavities and close to many hydrophobic amino acid residues. GLN68 and LEU49 were important amino acid residues for SnitCSP4 to bind various odors, and THR9 was the key ligand-binding site in identifying (-)-globulol in the SnitCSP4. Molecular dynamics verified the docking results, confirming that SnitCSP4 bound well to two sex pheromone molecules, three host plant volatiles, and three symbiotic fungal volatiles, with (Z)-7-heptacosene, (Z)-9-nonacosene, and (-)-globulol binding being the most highly stable. These results mean that SnitCSP4 is critical for insects recognizing scent molecules, providing a favorable molecular basis for regulating the behavioral interactions between *S. nitobei* and the environment, and offering the possibility of developing new strategies for more environmentally friendly and effective control.

Keywords: tissue-specific expression; binding characterization; molecular dynamics; molecular interaction; chemosensory protein; *Sirex nitobei*; volatiles

check for updates

Citation: Guo, P.; Hao, E.; Li, H.; Yang, X.; Lu, P.; Qiao, H. Expression Pattern, Molecular Docking and Dynamics Simulation Analysis of CSP4 from *Sirex nitobei* Provides Molecular Basis of CSP Bound to Scent Molecules. *Agronomy* **2022**, *12*, 1994. https://doi.org/10.3390/agronomy12091994

Academic Editors: Mario Contarini, Angelo Mazzaglia, Roberto Mannu and Luca Rossini

Received: 8 July 2022
Accepted: 18 August 2022
Published: 24 August 2022

Publisher's Note: MDPI stays neutral with regard to jurisdictional claims in published maps and institutional affiliations.

Copyright: © 2022 by the authors. Licensee MDPI, Basel, Switzerland. This article is an open access article distributed under the terms and conditions of the Creative Commons Attribution (CC BY) license (https://creativecommons.org/licenses/by/4.0/).

1. Introduction

Insects have developed an extremely sophisticated, sensitive, and specific olfactory system to detect, distinguish, interpret, and perceive various odorants from the environment [1,2]. In the insect chemosensory system, odorant binding proteins (OBPs) and chemosensory proteins (CSPs) can identify, capture, bind, and convey chemical odor molecules [3]. The complexes of OBP/CSP-odor molecules interact with chemosensory receptors found in the dendritic membrane of olfactory sensory neurons (OSNs) [4,5], followed by further signal transduction towards the olfactory neural center that stimulates physiological functions and behavioral responses in insects [6,7]. With the in-depth study of insect olfactory mechanisms, the concept of "reverse chemoecology" was proposed, which refers to the combination of OBPs or CSPs with odor molecules that can be used to screen for odor molecules with attractive or avoiding effects on insects, thus greatly reducing the workload of screening for active odor molecules.

CSPs are a class of soluble proteins consisting of 100–120 amino acid residues, generally with six α-helices forming a hydrophobic pocket and a signal peptide sequence consisting of the first 20 or so amino acid residues at the *n* terminus. They are typically characterized by the presence of four conserved cysteine (Cys) sites, which pair up to form two pairs of disulfide bonds used to keep the protein structure compact and stable [1,8–10]. More than a dozen orders of insects have been identified [11] since the first member of the CSP family was discovered more than a decade ago in Drosophila melanogaster and named olfactory specific protein D (OS-D) due to its preferential expression in the antennae [12], which are highly or specifically expressed in antennae and function as chemosignal receivers in the related studies [13]. For example, SinfCSP19 of Sesamia inferens was highly expressed in male antennae, which not only can effectively bind six host volatile components [14], but also express superb binding ability to three sex pheromone components, suggesting that SinfCSP19 was involved in host recognition of S. inferens. AlinCSP1-3 of Adelphocoris lineolatus, which are significantly expressed in antennae, can effectively bind odorant ligands such as Cis-3-Hexenol, *n*-Valeraldehyde and Methyl salicylate [15]. AgamCSP3, which is highly expressed in Anopheles gambiae antennae, can bind to pheromones [16]. These findings showed CSPs might play vital functions in chemical signal transduction. CSPs are commonly expressed in non-chemoreceptive tissues in addition to chemosensory tissues, which have a broader range of functions and research implications. Examples include pheromone-secreting glands [17], midgut [18], abdomen [19], reproductive organs [20], eggs [21], and feet [22], suggesting a non-olfactory role. In the praying mantis, CSP10 is involved in the regeneration of the broken foot of the mantis worm [12]. In honeybees, AmelCSP5 is associated with the development of fertilized eggs and epidermis [21,23]. Some other CSPs act as carriers of nutrient uptake and visual pigments in the beak and eyes of insects [24]. It has been shown that CSPs bind chemical pheromone signals in the gonads or reproductive organs and assist in their release into the environment [25–27]. Such a wide expression and binding profile of CSPs suggests that it plays a crucial role in the life activities of insects. Therefore, it is important to investigate the specific physiological functions of CSPs.

Sirex nitobei (Hymenoptera: Siricidae), native to Asia with a Palaearctic and Oriental distribution range, is an important wood-boring pest [28], causing the weakening and death of a considerable number of pines [29]. In China, the hosts of *S. nitobei* include *Pinus sylvestris* var. *mongolica*, *Pinus. tabuliformis*, *Pinus. armandii*, *Pinus. thunbergii*, and *Pinus. massoniana*, while in Japan, it infests *Pinus. densiflora* and *P. thunbergii* [30,31]. *S. nitobei* have been reported to carry *A. areolatum* and *A. chailletii* [32], which can also be considered a potentially high-risk invasive species that has attracted attention due to its sympatric coexistence with *S. noctilio*. Since it was first reported in China in 1980, the species has continued to expand its range and has spread into more than 10 provinces [33]. To prevent host death and economic loss, it has become particularly important to develop more effective prevention and control strategies. In *S. nitobei*, six CSPs were identified from antennal transcriptome analysis in the previous study [34], but there is no report on the tissue-specificity expression of CSP in *S. nitobei*. Moreover, its specific role in the olfactory system is uncertain and the molecular interaction mechanism is still not shown.

The present study was designed to characterize and identify *SnitCSP4* expression in *S. nitobei* based on a relatively high FPKM value obtained from the antennal transcriptome [34] and the role of a grid representation of SnitCSP4-ligands interactions after predicting the structural features and properties of the protein. We also intended to provide a basis for clarifying the chemosensory mechanism of *S. nitobei* and to guide the optimization of lure formulations.

2. Materials and Methods

2.1. Experimental Insects

S. nitobei-infested pine (*P. sylvestris var. mongolica*) logs were collected in Yushu City, Jilin Province (China, 44°50′20″ N, 126°32′6″ E) on 22 August 2020, and the logs sealed with wax were incubated in homemade mesh cages, controlled at 25 ± 1 °C and 60–70%

relative humidity in the laboratory. Adults were harvested within 3 days after emergence, marked for sex and date of emergence, then immediately frozen in liquid nitrogen and stored at −80 °C.

2.2. Total RNA Solation and First-Strand cDNA Synthesis

Different tissues (the antennae, heads, thoraxes, legs and external genitals) were separated quickly from 20 male and female adults after eclosion without mating, respectively, and three biological replicates were performed. Following the manufacturer's recommendations, total RNA was extracted from various tissues using the Trizol reagent (Invitrogen, Carlsbad, CA, USA) and the RNeasy Plus Mini Kit (Qiagen, Hilden, Germany). A NanoDrop ND-8000 spectrophotometer (NanoDrop products, Wilmington, DE, USA) was used to detect the concentration of extracted RNA, and 1% agarose gel electrophoresis was used to assess the quality of RNA extractions. First-strand cDNA was synthesized with a first-strand synthesis kit using PrimeScriptTM RT Reagent Kit with gDNA Eraser Kit (TaKaRa, Japan). The product was tested by 1% agarose gel electrophoresis and NanoDrop ND-8000, then stored at −20 °C for backup after being proven to be of good integrity and purity.

2.3. PCR Amplification and Sequence Analysis

Based on the *S.nitobei* antennal transcriptome sequencing data, SnitCSP4 (GenBank: QHN69083.1) sequence was obtained and identified by BLAST sequence comparison on the NCBI website. Gene-specific primer was designed to amplify the ORF sequence of the CSP gene. The first-strand cDNA (1 µL) was used as a template for PCR using a general protocol. The reaction mixture contained 12.5 µL of Premix, 0.5 µL of each degenerate primer and 10.5 µL of ddH_2O in a total volume of 20 µL. The PCR was carried out with the following conditions: initial preheating for 2 min at 95 °C, 34 cycles at 95 °C for 30 s, 55 °C for 30 s and 72 °C for 1 min, and with a final extension at 72 °C for 10 min, storing at 4 °C. The obtained PCR amplification products were sent to the company for sequencing. Primer synthesis and sequencing were completed by Rui Bo Xing Ke Biotechnology company (Beijing, China). Blast biological software (http://www.ncbi.Nlm.nih.gov/blast (accessed on 4 October 2021)) was used to perform similarity searches and sequence homology alignment. The SignalP5.0 (http://www.cbs.Dtu.dk/services/SignalP-5.0/ (accessed on 4 October 2021)) artificial neural network method predicted the existence of a signal peptide. The isoelectric point and molecular weight were predicted using the online program Expasy.

2.4. Tissue Expression Profile by qPCR

Specific primers used for qPCR were designed by the software Beacon Designer 7.90 (PREMIER Biosoft International) and are listed in Table 1. The reference gene, β-Tubulin was used for normalizing target gene expression and to correct for sample-to-sample variation. The first-strand cDNA (1 µL) was used as a template and each reaction was conducted in a 20 µL reaction mixture containing 1.0 µL of sample cDNA (150 ng), 10 µL of Mix (2×Taq PCR StarMix (TransGen Biotech, Beijing, China), 0.5 µL of forwarding primer (5 µM), 0.5 µL of reverse primer (5 µM), and 8 µL of nuclease free H_2O. The reaction programs were as follows: 95 °C for 30 s, followed by 40 cycles of amplification (95 °C for 5 s and 60 °C for 30 s). To find a single gene-specific peak and rule out primer dimer peaks, a melting curve for PCR products was examined. Non-template responses served as negative controls (replacing cDNA with H_2O). For each experiment, three biological and three technical replications were carried out. Relative quantification of different tissues was calculated by the comparative $2^{-\Delta\Delta Ct}$ method [35]. Using SPSS statistical software (version 26.0, SPSS Inc., Chicago, IL, USA) and one-way ANOVA tests, the target gene's comparative analysis across several tissues was determined ($p < 0.05$). The values are presented as the mean ± SE when appropriate.

Table 1. Primers used in qPCR.

Gene Name	Primers Sequence (5′→3′)	Annealing Temperature, °C	Segment Length, bp
SnitCSP4	F: ATTTCGAACAGCGCAGTTGG R: TCATCAAAGTCGGGCTTTCG	59.0	164
β-Tubulin	F: CGTCGGTTCCGTTGATAAGTTG R: AGAATATCCCGACCGAGTGTTG	59.0	122

2.5. Homologous Modeling and Models Evaluation

SWISS-MODEL is a fully automated protein structure homology modeling server via the ExPASy web server [36]. When the amino acid sequences were submitted to the SWISS-MODEL (https://www.Swissmodel.expasy.org/ (accessed on 5 December 2021)), the template selection, modeling, and optimization of homology models could be automatically carried out by the program. A template that meets the protein crystal structure requirements for CSP amino acid sequence identity greater than or equal to 30% and a template coverage of 90% or more was selected for modeling. Rationalization of the three-dimensional conformation of the protein using the online software SAVES 6.0 (https://saves.mbi.ucla.edu/ (accessed on 5 December 2021)), the model was analyzed and evaluated using Procheck, Verify 3D and ERRAT programs [37–39] to determine the rationality of the model and to observe the signature structural features.

2.6. Molecular Docking

A total of 14 ligands were screened for sex pheromones, host plant volatiles, and symbiotic fungal volatiles (Table 2), and their 3D structures (Figure 1) were downloaded by accessing the PubChem (https://pubchem.ncbi.nlm.nih.gov/ (accessed on 9 December 2021)) website on NCBI according to the names or CAS numbers. The files were converted to PDB format consistent with the candidate proteins by Pymol software. The binding energy of SnitCSP4 to 14 ligands was analyzed by Autodock 4.2.6 software that is a semi-flexible docking program for docking rigid receptor macromolecules with flexible ligand small molecules. Considering the sequence conservation of the protein with ligands, the binding site was confirmed for its hydrophobicity. The consensus score program and the score ligand posture program both examined and ranked these binding poses. Finally, complexes with the best 3D binding conformations were chosen and subjected to analysis and evaluation. Images were generated and further analyzed using PyMOL 2.2.0 software.

Table 2. Odor compound information used in docking.

Chemical Name	PubChem CID No.	Molecular Formula	Complex Code	Chemical Name	PubChem CID No.	Molecular Formula	Complex Code
Female Pheromones				*Male Pheromones*			
(Z)-7-heptacosene	56936088	$C_{27}H_{54}$	C_P-1	(Z)-3-dodecenol	5364626	$C_{12}H_{24}O$	C_P-3
(Z)-9-nonacosene	14367299	$C_{29}H_{58}$	C_P-2	(E,E)-2,4-decadienal	5283349	$C_{10}H_{16}O$	C_P-4
Host Plant Volatiles				*Symbiotic Fungi Volatiles*			
α-pinene	6654	$C_{10}H_{16}$	C_H-5	2-hexene	19966	C_6H_{12}	C_F-8
3-carene	26049	$C_{10}H_{16}$	C_H-6	terpene	6651	$C_{10}H_{20}O_2$	C_F-9
camphene	92221	$C_{10}H_{16}$	C_H-7	6-methyl-5-hepten-2-one	9862	$C_8H_{14}O$	C_F-10
				Trans-3-hexenyl acetate	5352557	$C_8H_{14}O_2$	C_F-11
				Linalool	6549	$C_{10}H_{18}O$	C_F-12
				Geraniol	637566	$C_{10}H_{18}O$	C_F-13
				(-)-globulol	12304985	$C_{15}H_{26}O$	C_F-14

C_P, C_H, and C_F refer to the complexes of SnitCSP4 and sex pheromones, the complexes of SnitCSP4 and host plant volatiles, and the complexes of SnitCSP4 and symbiotic fungi volatiles, respectively.

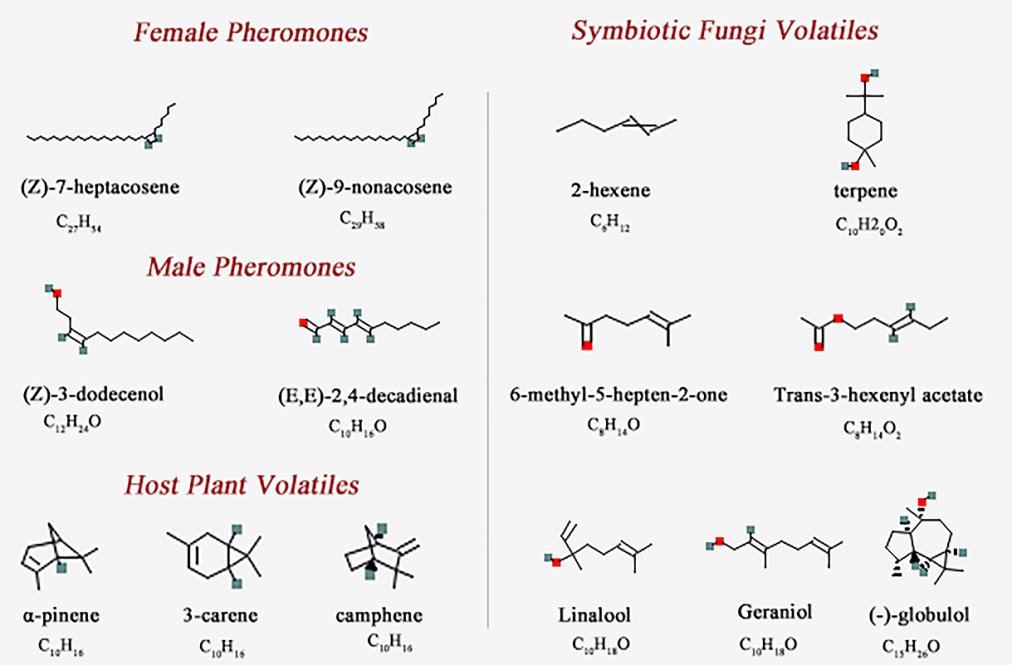

Figure 1. The 2D structures of 14 ligands.

2.7. Molecular Dynamics

After obtaining protein conformation as described above, Gromacs 2019.6 package [40] was then employed to simulate each complex with the AMBER-ff99sb-ildn force field [41] for SnitCSP4 and the AmberTools 18 GAFF force field [42], which was optimized with the ACPYPE script [43] for Ligands. Ligand information is listed in Table 2. Transferable interatomic potential with three-point model (TIP3P) water molecules was used to solvate the docked complex, and Cl^- and Na^+ were added to neutralize the system. Then we performed energy minimization using the conjugated gradient (CG) method to make the maximum energy of the system less than 1000 $kJ \cdot mol^{-1} \cdot nm^{-1}$. Thereafter, each protein-ligand complex was equilibrated using canonical (NVT) and isothermal-isobaric (NPT) ensembles. Finally, utilizing a V-rescale thermostat and a Parrinello–Rahman barostat, this pre-equilibrated system was subjected to a 40-ns molecular dynamics (MD) simulation [44] with a time interval of 2 fs and specific heat (298.15 K) and pressure (1 bar) coupling. All analysis of results was performed using Gromacs 2019.6 package.

3. Results

3.1. Sequence Analysis of SnitCSP4

The sequencing results showed that the open reading frame (ORF) of SnitCSP4 was 396 bp, encoding 131 amino acids (Figure 2). The various properties of the protein are shown in Table 3. The instability index (II) of 38.08 showed that SnitCSP4 is relatively stable and the grand average of hydropathicity (GRAVY) was −0.330, indicating that it is a hydrophilic protein. Among the 20 amino acids comprising the protein, lysine (Lys) has the highest percentage at 11.5%. In addition, the amino acid sequences of SnitCSP4 contain four conserved cysteine sites, which is consistent with the protein family of CSPs. After searching the NCBI database, the sequence similarity of SnitCSP4 only exceeded 60% with SnocCSP4, Ssp.CSP7, and SguaCSP1, with 98.23%, 66.37%, and 65.49%, respectively, which clearly showed that there is a large difference in terms of consistency among the sequences of CSP genes.

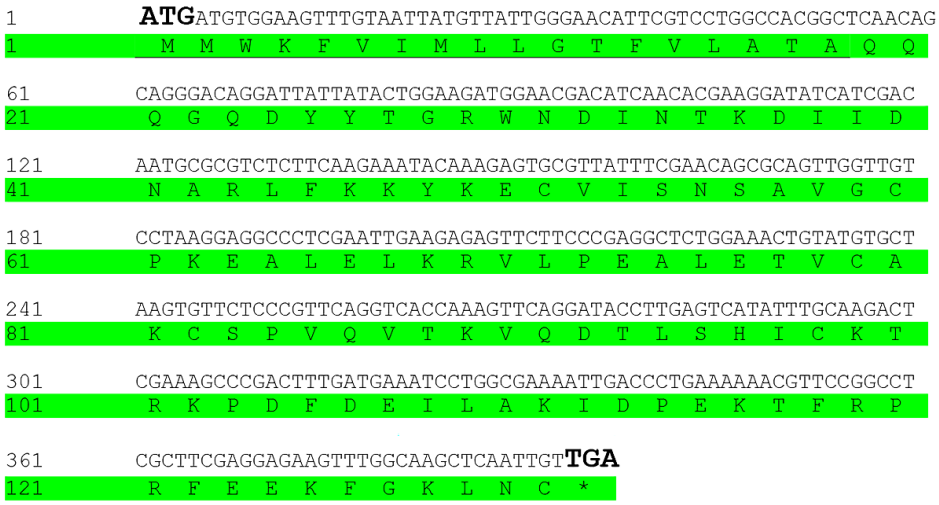

Figure 2. Nucleotide and deduced amino sequences. The start and stop codons are shown in bold type, the asterisk marks the translation termination codon, and the predicted signal peptide is underlined.

Table 3. Information on the biochemical properties of SnitCSP4.

Name	Molecular Formula	MW (ku)	pI	Aliphatic Index	Instability Index	GRAVY
SnitCSP4	$C_{675}H_{1079}N_{179}O_{193}S_9$	15.08	8.73	82.60	38.08	−0.330

3.2. Tissues-Specificity Expression Analysis

SnitCSP4 was expressed in antennae, head, thorax, external genitalia, and feet (Figure 3). Notably, there was significant expression in the female antennae and over 300 times more than in the female thorax, suggesting an association with the olfactory behavior of *S. nitobei*. There were significant differences in male and female antennae, showing a certain sex difference. Additionally, *SnitCSP4* was also highly expressed in the male external genitalia, indicating that it may have a specific function in the external genitalia of *S. nitobei*, laying an experimental foundation for further studies later.

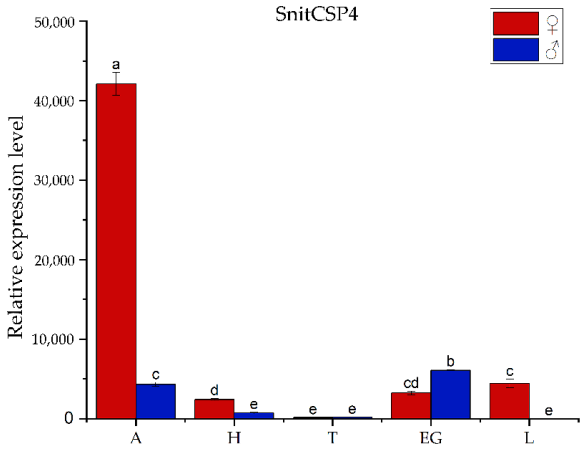

Figure 3. Transcript levels of tissue-specific CSP gene in different tissues of *S. nitobei*. A, antennae; H, head (without antennae); T, thorax; EG, external genitalia; L, leg. Red indicates expression in females and blue indicates expression in males. The reference gene, β-tubulin was used for normalizing CSP genes expression and to correct for sample-to-sample variation. Transcript levels were normalized to those of FT. The standard error is represented by the error bar, and the different lower cases above each bar indicate significant differences ($p < 0.05$).

3.3. Homology Modeling Analysis

To construct the valid model, the crystal structure of CSP6 in *Mamestra brassicae* (PDB ID:1N8U, chain A) was selected as the most satisfactory template, which had a sufficient homology for SnitCSP4 (sequence identity > 30.0%) (Figure 4A). After modeling, the final model of SnitCSP4 (Figure 4B) satisfying the rationality verification was obtained for further experiments. In the Ramachandran plot (Supplementary Figure S1a), 91.3% (>90%) of amino acid residues were located in the most favored regions, implying good stereochemical quality of the constructed SnitCSP4 model. Moreover, 94.12% (>90%) of the amino acid residues had tertiary structures scores above 0.2 (Supplementary Figure S1b), and the overall quality factor of ERRAT was 100% (Supplementary Figure S1c) of the non-covalent interactions between different atom types of SnitCSP4, which is much higher than 50% of the reliable con-formational values, indicating that the overall non-covalent bond interactions in SnitCSP4 are reasonable. The above exactly proved the reliability of the model.

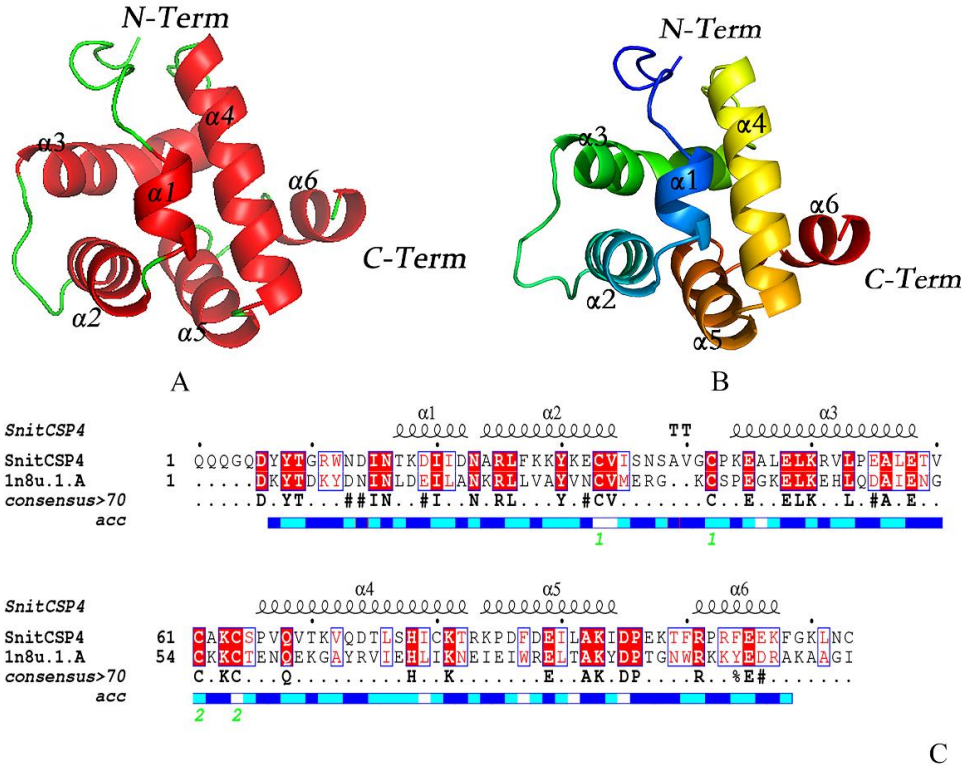

Figure 4. The 3D structure of SnitCSP4. (**A**) Structural modeling of SnitCSP4; (**B**) Corresponding modeling template of SnitCSP4; (**C**) Sequence comparison of SnitCSP4 with its modeling template. The six α-helices are marked as α1-α6. C-term and N-Term are abbreviations for C-terminus and N-terminus, respectively.

The 3D structure of SnitCSP4 resembles a sphere with an exterior covered with hydrophilic amino acids and consists of six conically arranged α-helices (α1-α6) (Figure 4B). Of the six helices, α2 and α3, α3 and α4 are connected in pairs by two disulfide bonds formed between four conserved cysteines (Cys51- Cys60, Cys79- Cys82). These disulfide bonds are believed to stabilize the right conformation of SnitCSP4.

3.4. Molecular Docking Analysis

The binding energy reflects the binding between the receptor proteins and ligand molecules. In this study, SnitCSP4 had a more concentrated and less variable binding energy distribution with the same source ligands, except for the symbiotic fungal volatiles, and had lower binding energy with female pheromones than the other two types of

odorants (Figure 5). For the symbiotic fungal volatiles, the binding energy fluctuated greatly, with the highest binding energy of −3.19 kJ/mol for 2-hexene and the lowest binding energy of −7.06 kJ/mol for (-)-globulol, indicating that SnitCSP4 has a stronger affinity for some specific fungal volatiles and even bound better than female pheromones. Overall, SnitCSP4 bound better to two pheromones, three host plant volatiles, and three symbiotic fungal volatiles, with the better binding being the female pheromone components (Z)-7-heptacosene, (Z)-9-nonacosene, and the symbiotic fungal volatile (-)-globulol.

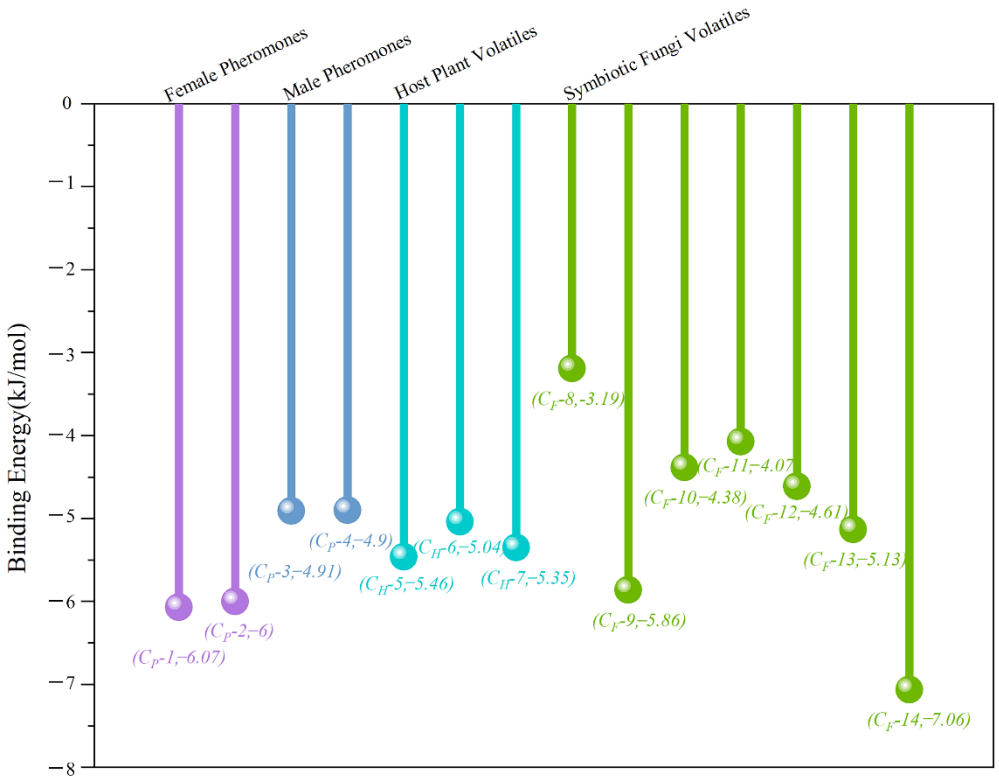

Figure 5. Binding energy of 14 ligands docked to the SnitCSP4 model.

(Z)-7-heptacosene is a long carbon chain molecule, and it entered the interior of the binding cavity in the form of a coiled fold and bound more tightly to SnitCSP4 mainly by intermolecular forces (Figure 6A,D). ILE20, TYP30, ILF15, ALA46, GLU45, GLU48, TRP12, GLN68, CYS64, TYR8, CYS61, LEU53, LEU49, VAL52, ALA56, THR75, ILE90, and PHE27 were the action sites of van der Waals. VAL72, LYS71, LEU76, and ILE79 were the action sites of alkyl interactions (Figure 7A). These amino acid residues constituted the cavities and grooves on the surface of SnitCSP4, which formed the basis for the interaction.

(Z)-9-nonacosene is also a long carbon chain molecule, so the binding to SnitCSP4 was relatively similar to that of (Z)-7-heptacosene. (Z)-9-nonacosene disc region folded into the interior of the binding cavity (Figure 6B,E), and the amino acid residues forming van der Waals forces with (Z)-9-nonacosene were GLN68, LYS71, VAL72, LEU49, LEU53, TYR30, ILE20, THR75, LEU76, PHE27, LYS31, VAL34 ILE90, VAL52, ALA56, LEU57, CYS61, and VAL60. The amino acid residues that formed Pi-interaction were PHE104, PHE100 (Figure 7B).

(-)-globulol bound inside the binding cavity of SnitCSP4 and bound tightly to it (Figure 6C,F). ILE15, GLN68, ASN13, ARG11, GLY10, GLU48 and GLU45 were the action sites of van der Waals. LYS71, VAL72, LEU49, VAL52, and TYR8 were the action sites of hydrophobic interaction. THR9 formed the hydrogen bond with bond lengths of 2.71 Å (Figure 7C), respectively. Hydrogen bonding is a strong intermolecular force that makes the binding of proteins to ligands stronger and more stable, indicating that THR9 is key site for the binding of SnitCSP4 to (-)-globulol.

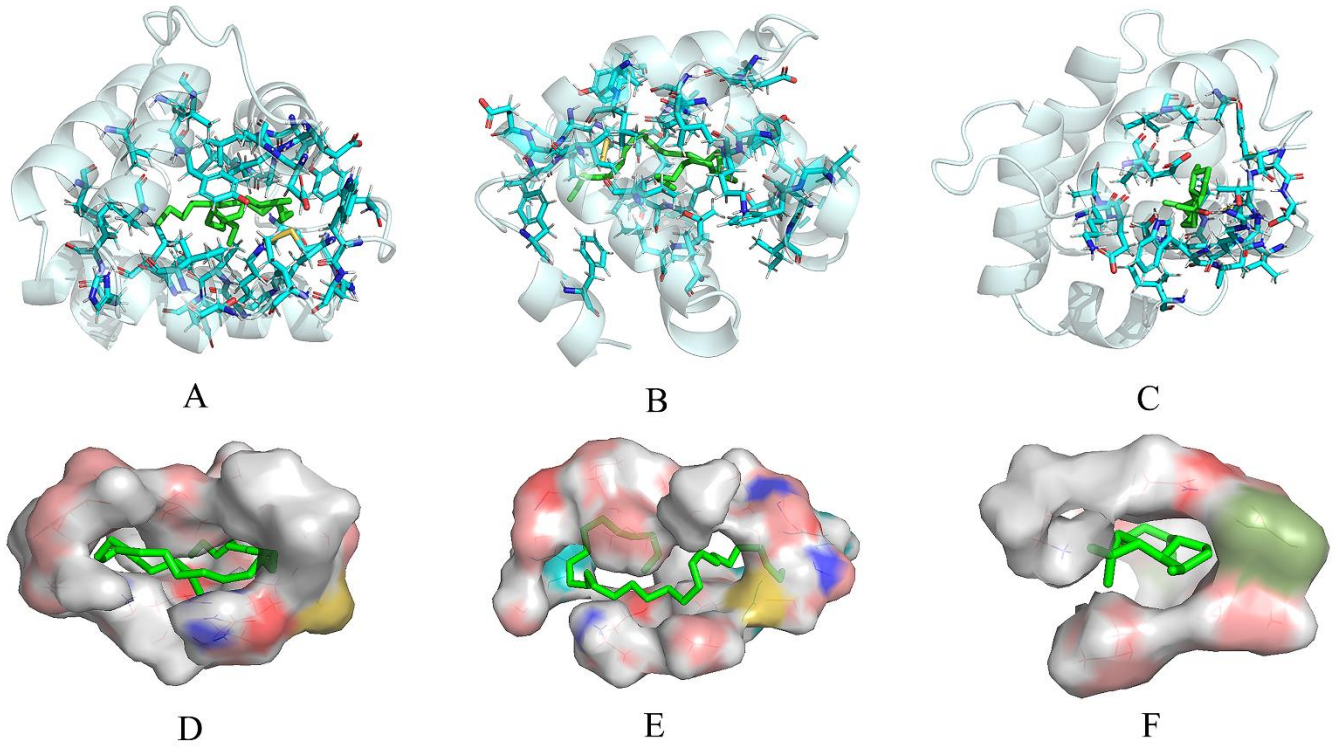

Figure 6. Binding pattern of SnitCSP4. (**A**–**C**) The 3D structure of SnitCSP4 and (Z)-7-heptacosene, (Z)-9-nonacosene, (-)-globulol. (**D**–**F**) Detailed binding pattern of the corresponding distal pocket of the protein-ligand complex.

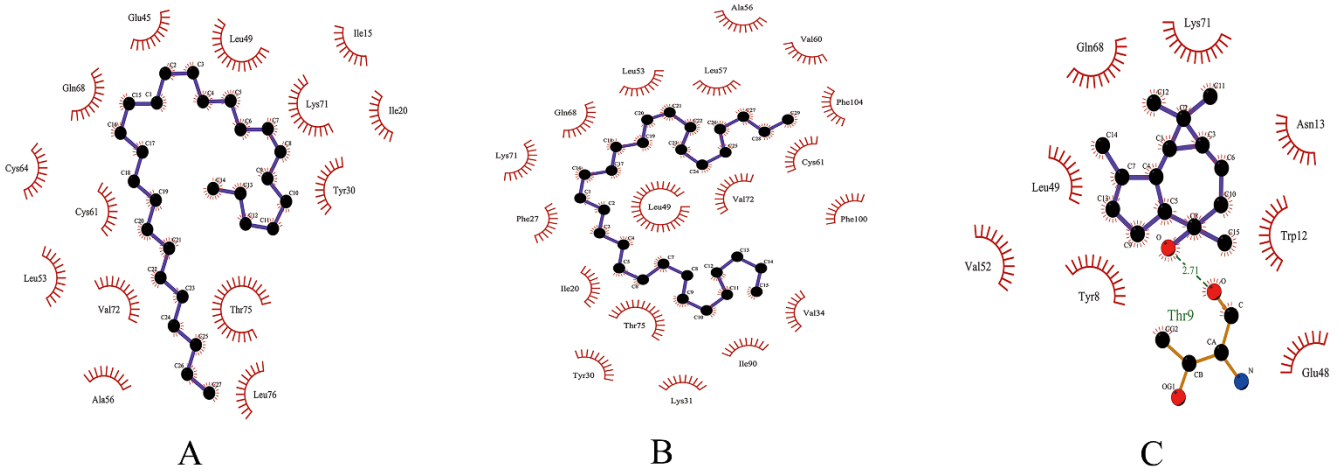

Figure 7. Interactions in protein-ligand binding complexes. (**A**) SnitCSP4-(Z)-7-heptacosene, (**B**) SnitCSP4-(Z)-9-nonacosene, (**C**) SnitCSP4-(-)-globulol complexes.

The docking models in this study showed that all odor molecules bound in the hydrophobic cavities and were near many hydrophobic amino acid residues. Two hydrophobic amino acid residues, GLN68 and LEU49, interacted with all ligands, and the above results suggested that GLN68 and LEU49 were the important amino acid residues for SnitCSP4 to bind to various odor molecules and THR9 was the key ligand-binding site on identifying (-)-globulol in the SnitCSP4.

3.5. Stability of SnitCSP4-Ligand Complexes in MD Simulation

Fourteen odor ligands were docked with SnitCSP4, and molecular dynamics (MD) simulations were performed for the resulting 14 complexes. MD simulations are computer models of molecular motion, which have great significance to analyze the internal motions and stability of protein-ligand complexes. According to the time-evolution RMSD curves of 14 systems, almost all docked complexes achieved an equilibrium of about 10 ns with different average RMSD, and all systems converged within 40 ns, demonstrating the usefulness and applicability of 40 ns MD simulations as a base for examining the global conformation. The average RMSD value of the 14 systems ranged from 0.27 nm to 0.40 nm. The maximum value of the standard deviation of the RMSD was 0.04 nm, and the minimum value was only 0.01 nm (Figure 8).

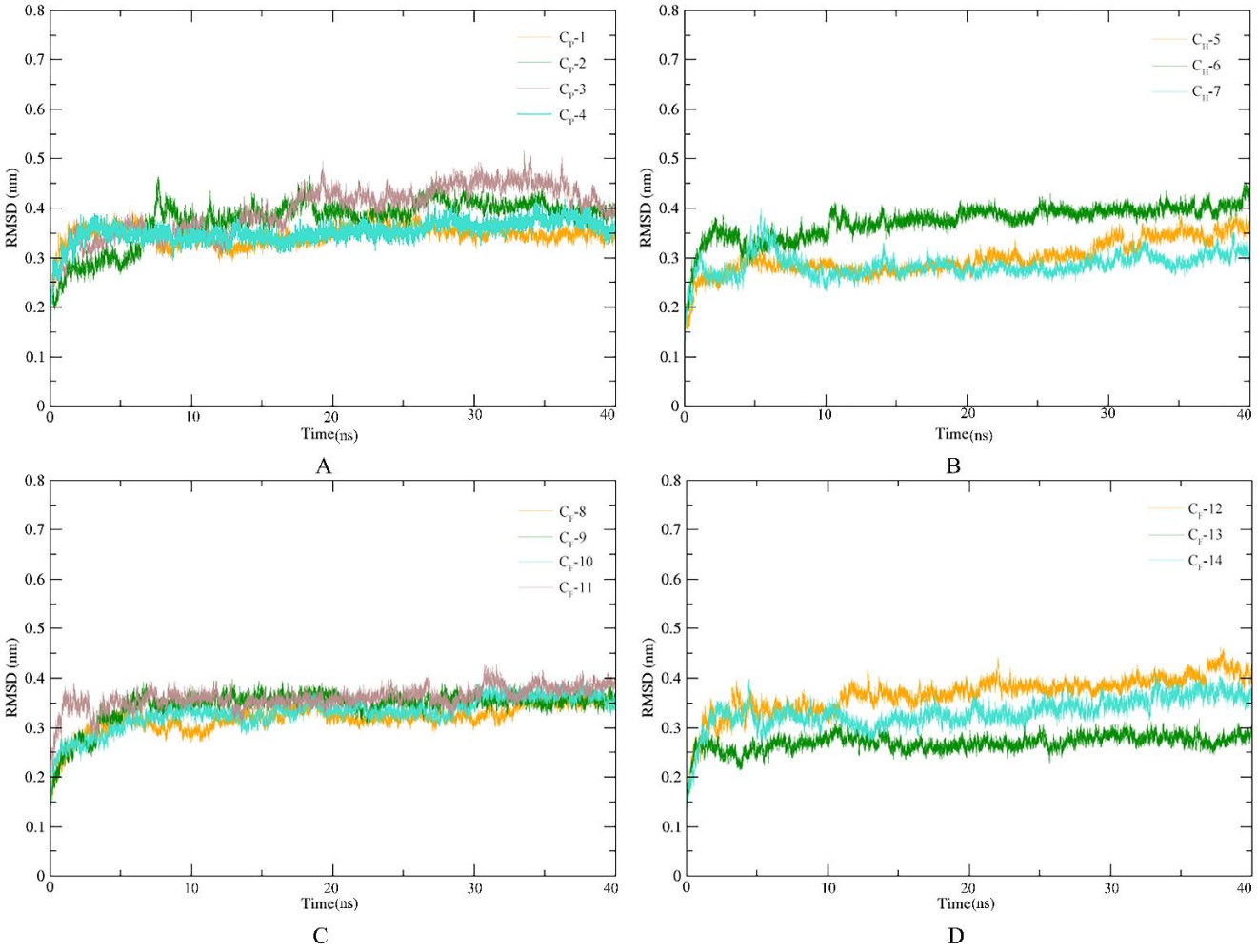

Figure 8. The root-mean-square deviation (RMSD) value for carbon backbones of SnitCSP4-ligand complexes during the 40 ns molecular dynamics (MD) simulations. (**A**) RMSD of C_P-1, C_P-2, C_P-3, C_P-4; (**B**) RMSD of C_H-5, C_H-6, C_H-7; (**C**) RMSD of C_F-8, C_F-9, C_F-10, C_F-11; (**D**) RMSD of C_F-12, C_F-13, C_F-14.

Flexibility and local motion characters of the 14 complexes were further measured by the value of root-mean-square deviation (RMSF). As a whole, the 14 complexes exhibit similar motions during the 40 ns MD simulations (Figure 9). There are three major regions with more sharp fluctuations, including residues 25 (α2 helix), 39–41 (loop at the front of the α3 helix), and 106–108 (near the C-terminus), where the loop has little effect on the binding interface of the complex because it is far from the ligand-binding site (Figure 6), while the four hydrophobic residues (ARG25, GLU106, LYS107 and PHE108) are very close

to the ligand-binding site. In these regions, poor stability of their SnitCSP4-ligand complex interactions leads to drastic fluctuations. A relatively stable region in the RMSD diagram can be seen at residues 29–36, which are notably still very close to the binding site in the α3 helix. It is speculated that their presence is a key factor in maintaining the stability of SnitCSP4-ligand binding. The average value of RMSF is around 1.7 nm in both C_P-1 and C_P-2 (Figure 9). However, in the case of both C_P-3 and C_P-4, the average value of the RMSF is around 0.21 nm, and even more frequent fluctuations can be noticed, indicating poor stability. For C_H-5, C_H-6, C_H-7, C_F-9, C_F-13, and C_F-14, instead, smaller spikes can be observed (Figure 9), suggesting the relative stability of the complexes, which is in general agreement with the previous molecular docking results.

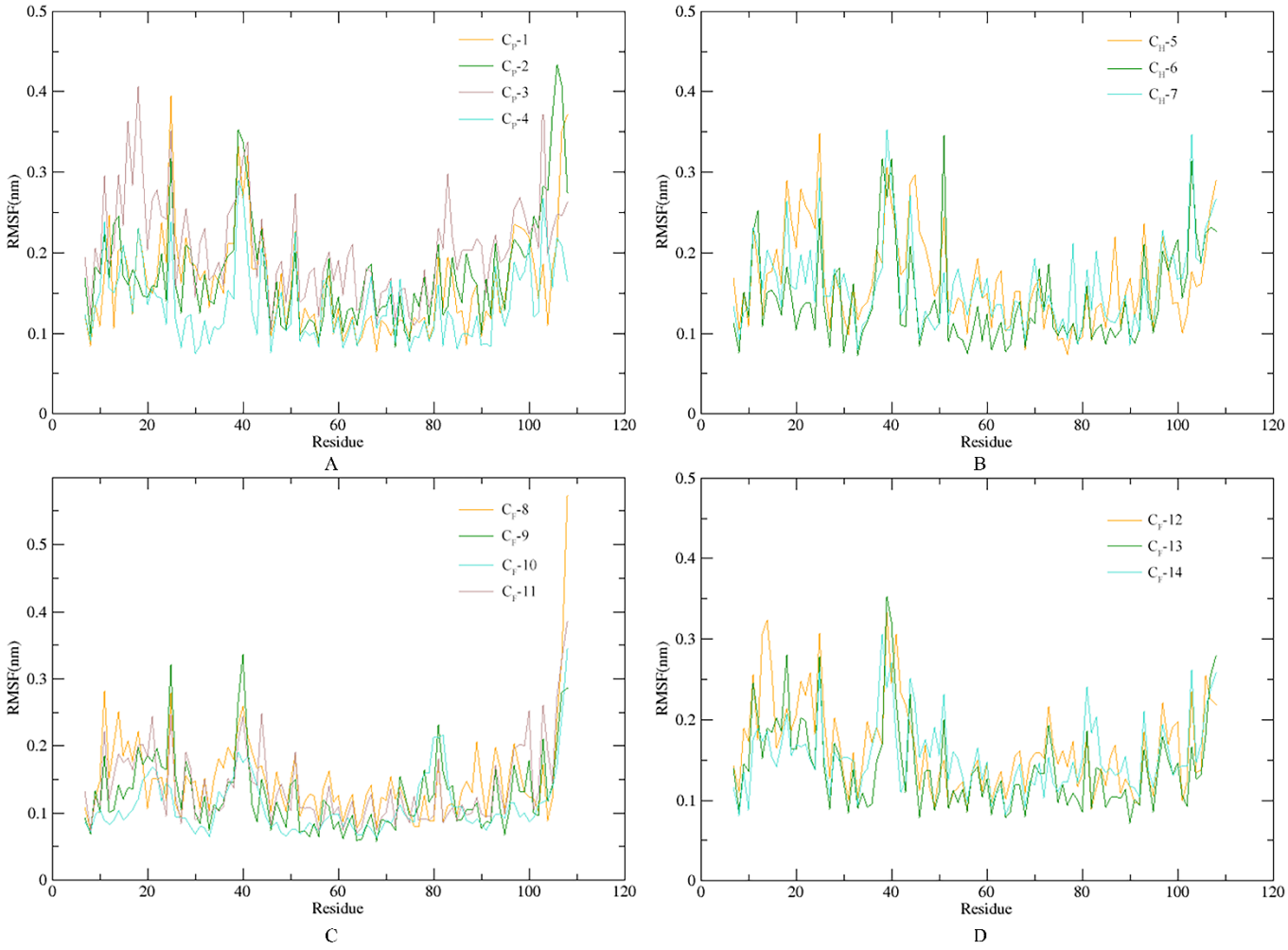

Figure 9. Residue fluctuations for SnitCSP4-ligand complexes during 40 ns MD simulations. (**A**) RMSF of C_P-1, C_P-2, C_P-3, C_P-4; (**B**) RMSF of C_H-5, C_H-6, C_H-7; (**C**) RMSF of C_F-8, C_F-9, C_F-10, C_F-11; (**D**) RMSF of C_F-12, C_F-13, C_F-14.

4. Discussion

Insects mainly use their antennae to detect chemical odorants in the environment. Different olfactory receptors in the antennae play a crucial role in host plant recognition and mate selection. *CSPs* are specifically expressed only in the antennae of *Polistes dominula*, *Linepithema humile*, and *Vespa crabro*, suggesting a possible specific function of CSP in these three Hymenoptera [45,46]. Si-CSP of *Solenopsis invicta* bound strongly to polar epidermal lipid-like molecules and was specifically expressed in the dilated nodes at the end of worker bees' antennae, where the porous olfactory sensors were almost entirely distributed, suggesting that the CSP was involved in the perception of volatile chemical stimuli in

red fire ants [47]. Our qRT-PCR results revealed *SnitCSP4* was significantly expressed on the female antennae, thus it is hypothesized that SnitCSP4 has specific functions in the antennae and is involved in olfactory sensory behaviors such as locating host plants for egg-laying sites and recognizing other external chemical odorants. In addition, female antennae show much higher expression than male. *CSP2* and *CSP3* of *Microplitis mediator* as well as *CSP1* and *CSP3* of *Chouioia cunea* were mainly expressed in the antennae, and the expression of *CcunCSP3* in the female antennae was significantly higher than that in the male antennae [48,49], presenting a certain gender expression difference, which was consistent with the expression pattern of *SnitCSP4*. Notably, the CSP gene highly expressed in antennae may play a vital role in the recognition of sex pheromones and common odor molecules. An in-depth study of the functions of the CSP could help us elucidate the molecular mechanisms of *S. nitobei* communication and could serve as target genes for interfering with insect olfactory recognition.

We delved into the crystal structure and ligand binding properties of the protein to precisely reveal the specific mechanisms underlying the binding of CSP to odor molecules. By molecularly docking SnitCSP4 with 14 ligands, we found that two amino acids, GLN68 and LEU49, formed certain interactions with all ligands during the docking process, indicating that they are necessary for the binding. It is noteworthy that the binding of various ligands was remarkably different, which may be caused by specific amino acids located in the hydrophobic cavity, For example, in the CSPsg4, the IIE76 and TRP83 are involved in oleamide binding [50], in the CSPMbraA6, TYR26 plays a key role in the binding of 12-bromo-dodecanol ($BrC_{12}OH$) [51]. So, those amino acid residues located in the binding pocket of SnitCSP4, such as lysine, glutamate, tyrosine, arginine, leucine, threonine, valine, isoleucine, glutamine, phenylalanine, may also be involved in the recognition and binding of the hydrophobic ligands.

SnitCSP4 has binding affinity for most of the compounds tested. Among the 14 ligands, we identified two sex pheromone molecules, three host plant volatiles, and three symbiotic fungal volatiles with higher binding affinity, with (Z)-7-heptacosene, (Z)-9-nonacosene, and (-)-globulol binding most highly stable. In a molecular docking and molecular dynamics study of SnocOBP7 with 11 odorant molecules, Li et al. found that SnocOBP7 bound most stably to (Z)-7-heptacosene, (Z)-7-nonacosene and (-)-globulol [52], which was consistent with our results. In the study of the interaction mechanism of RpadOBP3 from *Rhopalosiphum padi* with (E)-β-farnesene(EβF), Fan identified three amino acid residues in the hydrophobic structural domain, TRP71, TRP68, and PHE2, bound tightly to EβF [53]. Tian et al. predicted the affinity of 31 odorant molecules by 3D modeling and molecular docking of *Cydia pomonella* sex pheromone binding protein (CpomPBP2) and found that CpomPBP2 had the highest affinity with 1-dodecanol [54]. Venthur et al. predicted the binding mechanism of the complex using molecular docking and molecular dynamics simulations of *Lobesia botrana* sex information binding protein (LbotPBP1) with 11 sex pheromone molecules and six host volatiles, and found that 11-dodecenyl was the best ligand for LbotPBP1 [55]. Our findings indicated that SnitCSP4 plays an important role in the olfactory behavior of *S. nitobei*, and as a result, we intend to further research to discover particular physiological behavioral reactions that occur when SnitCSP4 binds to odor molecules in the environment.

S. nitobei congregate in the same region of the top canopy during mating because they enjoy light, are most concentrated at 26–30 °C, and have strong flight abilities [56], To maximize the chance of a successful mating, males and females must find one another after meeting in the high canopy via a variety of signals. (Z)-7-heptacosene and (Z)-9-nonacosene are most likely scent substances used by males to locate females. In a related study on *S. noctilio*, it was found that males always approached the rear of females before mating and touched the ends of females' bodies with their genitalia [57], indicating that males use their genitalia to recognize females, demonstrating a distinct interaction behavior regulated by odor molecules, which was corroborated by our previous study on the high expression of *SnitCSP4* in the male external genitalia. These female pheromones could therefore direct the

creation of attractants. α-pinene and camphene are volatiles released by *Pinus sylvestris var. mongolica* [58], which were reported as the main host plants of *S. nitobei* [59]. 3-carene was a volatile of *P. Sylvestris* [60]. α-pinene, camphene, and 3-carene were used as plant-derived trap cores for forest behavior experiments and trapped a large number of *Sirex. noctilio* [61], a closely related species of *S. nitobei*. In China, *S. nitobei* was found to co-infest host plant species together with *S. noctilio* [62], which started to emerge in the field from late June to early September. Subsequently, a peak of *S. nitobei* was found to emerge during late August and late September from the same trees. In this study, these three ligands showed a relatively high binding affinity with SnitCSP4, further supporting the potential function of SnitCSP4 in host recognition.

We could not exclude other roles the CSP might play in the *S. nitobei*. The identification of CSP in different tissues indicated that these proteins perform different functions. The CSP genes from *Eogystia hippophaecolus* (EhipCSP4 and EhipCSP11) were found to be highly expressed in the external genitalia ($p < 0.01$) and were suggested to be involved in mate positioning or mating activities [63]. In the honey bees, the AmelCSP5 was found only in the ovaries and eggs of queen bees and in no other adult or larval body parts were they observed, suggesting a crucial role in the development of fertilized eggs [21,23]. In the *Periplaneta Americana* (American cockroach), a CSP like gene named P10 was expressed 30 times more in the regenerating legs than in normal legs, indicating P10 gene may be devoted to the regeneration of insect legs [12,22]. CSPs expressed in the proboscis, antennae, and pheromonal glands of cabbage armyworm, *Mamestra brassicae*, bound with sex pheromone analogues, suggesting that these CSPs are involved in pheromone detection [27,64].

The symbiotic fungi of *S. nitobei* are *A. areolatum* and *A. chailletii.* During egg laying the female adult injects eggs and mycelial fragments of the symbiotic fungus stored in the storage capsule into the host plant [32], and the lignocellulase secreted by the symbiotic fungus promotes the decomposition of the plant xylem for the larvae to feed on [65,66], hastening the host plant's death [67]. The binding affinity of (-)-globulol was by far the highest of the investigated symbiotic fungus volatiles. According to some studies, (-)-globulol was significantly attractive to female *S. noctilio* [68], and as its close relative, male *S. nitobei* may favor flying to locations with high concentrations of symbiotic fungal volatiles because these areas may have weaker host plants and greater resources for mating. Tissue-specific expression experiments revealed that *SnitCSP4* was expressed in the external genitalia of males, subsequent molecular docking and dynamics simulation studies showed that (-)-globulol were able to bind strongly to SnitCSP4, which could be connected to the mating behavior of adult males. The protein bound to (-)-globulol and other symbiotic fungal volatiles to signal the possible presence of females to other males. As a result, it may be able to regulate the behavioral interaction between males and the environment by controlling the amount of (-)-globulol.

Based on the property of *S. nitobei* to find suitable egg-laying locations through symbiotic fungi, further mixing of symbiotic fungal volatiles into plant-derived, pheromone lure cores can be attempted to efficiently trap female wasps trying to lay eggs. The simulation analysis of the ligand-binding interactions of SnitCSP4 allows for the development of innovation to prevent the reproduction of *S. nitobei* by intervening during the courtship period. Thus, we can trap them efficiently to reduce the population density and green control can be achieved. The above findings are of great importance for revealing the molecular mechanism of odor recognition by *S. nitobei* and for enriching the theory of *S. nitobei* chemoecology. A comprehensive and systematic understanding of the role of the protein in the life activities of *S. nitobei* is needed to better control their harmful range and reduce economic and ecological losses.

Supplementary Materials: The following are available online at https://www.mdpi.com/article/10.3390/agronomy12091994/s1, Figure S1: Quality evaluation of the CSP4 model.

Author Contributions: E.H. conceptualized and proposed the study idea; investigation, P.G. carried out the required biochemical experiments with the help of H.L.; P.G., and E.H. carried out the bioinformatics, molecular docking, and molecular dynamics experiments; methodology, E.H. and P.L.; formal analysis, P.G. and H.L.; resources, P.L., H.Q., and X.Y.; software, E.H. and X.Y.; writing—original draft preparation, P.G. and E.H.; writing—review and editing, P.G., E.H., P.L. and H.Q. All authors have read and agreed to the published version of the manuscript.

Funding: This research was supported by the National Natural Science Foundation of China (Grant No. 31570643, 81774015), the National Key R&D Program of China (2017YFD0600103), and the National Undergraduate Training Programs for Innovation and Entrepreneurship (202110022007). The funders had no role in study design, data collection and analysis, decision to publish, or preparation of the manuscript.

Institutional Review Board Statement: Not applicable.

Informed Consent Statement: Not applicable.

Data Availability Statement: The authors confirm that the data supporting the findings of this study are available within the article and its Supplementary Materials.

Acknowledgments: We thank anonymous reviewers and editors for their comments and suggestions on the manuscript.

Conflicts of Interest: The authors declare no conflict of interest.

References

1. Pelosi, P.; Zhou, J.J.; Ban, L.P.; Calvello, M. Soluble Proteins in Insect Chemical Communication. *Cell. Mol. Life Sci.* **2006**, *63*, 1658–1676. [CrossRef] [PubMed]
2. van der Goes van Naters, W.; Carlson, J.R. Insects as Chemosensors of Humans and Crops. *Nature* **2006**, *444*, 302–307. [CrossRef] [PubMed]
3. Fleischer, J.; Pregitzer, P.; Breer, H.; Krieger, J. Access to the Odor World: Olfactory Receptors and Their Role for Signal Transduction in Insects. *Cell. Mol. Life Sci.* **2018**, *75*, 485–508. [CrossRef] [PubMed]
4. Leal, W.S. Pheromone Reception. In *The Chemistry of Pheromones and Other Semiochemicals II*; Schulz, S., Ed.; Springer: Berlin/Heidelberg, Germany, 2005; pp. 1–36. ISBN 978-3-540-31477-6.
5. Leal, W.S. Odorant Reception in Insects: Roles of Receptors, Binding Proteins, and Degrading Enzymes. *Annu. Rev. Entomol.* **2013**, *58*, 373–391. [CrossRef] [PubMed]
6. Antony, B.; Soffan, A.; Jakše, J.; Abdelazim, M.M.; Aldosari, S.A.; Aldawood, A.S.; Pain, A. Identification of the Genes Involved in Odorant Reception and Detection in the Palm Weevil Rhynchophorus Ferrugineus, an Important Quarantine Pest, by Antennal Transcriptome Analysis. *BMC Genom.* **2016**, *17*, 69. [CrossRef]
7. Pelosi, P. Diversity of Odorant-Binding Proteins and Chemosensory Proteins in Insects. *Chem. Senses* **2005**, *30*, i291–i292. [CrossRef] [PubMed]
8. Angeli, S.; Ceron, F.; Scaloni, A.; Monti, M.; Monteforti, G.; Minnocci, A.; Petacchi, R.; Pelosi, P. Purification, Structural Characterization, Cloning and Immunocytochemical Localization of Chemoreception Proteins from Schistocerca Gregaria. *Eur. J. Biochem.* **1999**, *262*, 745–754. [CrossRef]
9. Jin, R.; Liu, N.; Liu, Y.; Dong, S. A Larval Specific OBP Able to Bind the Major Female Sex Pheromone Component in Spodoptera Exigua (Hübner). *J. Integr. Agric.* **2015**, *14*, 1356–1366. [CrossRef]
10. Zhang, T.; Wang, W.; Zhang, Z.; Zhang, Y.; Guo, Y. Functional Characteristics of a Novel Chemosensory Protein in the Cotton Bollworm Helicoverpa Armigera (Hübner). *J. Integr. Agric.* **2013**, *12*, 853–861. [CrossRef]
11. Li; Gu, T.; Chen, C.; Huang, K.; Tian, S.; Zhao, X.; Hao, D. CDNA Cloning, Sequence Analysis and Expression Profie of a Chemosensory Protoin from the *Clostera Restitura* (Lepidoptera:Notodontidae). *Sci. Silvae Sin.* **2018**, *54*, 67–75. [CrossRef]
12. Nomura Kitabayashi, A.; Arai, T.; Kubo, T.; Natori, S. Molecular Cloning of CDNA for P10, a Novel Protein That Increases in the Regenerating Legs of Periplaneta Americana (American Cockroach). *Insect Biochem. Mol. Biol.* **1998**, *28*, 785–790. [CrossRef]
13. He, P.; Li, Z.-Q.; Zhang, Y.-F.; Chen, L.; Wang, J.; Xu, L.; Zhang, Y.-N.; He, M. Identification of Odorant-Binding and Chemosensory Protein Genes and the Ligand Affinity of Two of the Encoded Proteins Suggest a Complex Olfactory Perception System in Periplaneta Americana: Cockroach Odorant Binding and Chemosensory Protein. *Insect Mol. Biol.* **2017**, *26*, 687–701. [CrossRef] [PubMed]
14. Zhang, Y.-N.; Ye, Z.-F.; Yang, K.; Dong, S.-L. Antenna-Predominant and Male-Biased CSP19 of Sesamia Inferens Is Able to Bind the Female Sex Pheromones and Host Plant Volatiles. *Gene* **2014**, *536*, 279–286. [CrossRef] [PubMed]
15. Gu, S.-H.; Wang, S.-Y.; Zhang, X.-Y.; Ji, P.; Liu, J.-T.; Wang, G.-R.; Wu, K.-M.; Guo, Y.-Y.; Zhou, J.-J.; Zhang, Y.-J. Functional Characterizations of Chemosensory Proteins of the Alfalfa Plant Bug Adelphocoris Lineolatus Indicate Their Involvement in Host Recognition. *PLoS ONE* **2012**, *7*, e42871. [CrossRef]

16. Iovinella, I.; Bozza, F.; Caputo, B.; Della Torre, A.; Pelosi, P. Ligand-Binding Study of Anopheles Gambiae Chemosensory Proteins. *Chem. Senses* **2013**, *38*, 409–419. [CrossRef]
17. Dyanov, H.M.; Dzitoeva, S.G. Method for Attachment of Microscopic Preparations on Glass for in Situ Hybridization, PRINS and in Situ PCR Studies. *Biotechniques* **1995**, *18*, 822–824, 826.
18. Singh, S.; Tyagi, C.; Rather, I.A.; Sabir, J.S.M.; Hassan, M.I.; Singh, A.; Singh, I.K. Molecular Modeling of Chemosensory Protein 3 from Spodoptera Litura and Its Binding Property with Plant Defensive Metabolites. *IJMS* **2020**, *21*, 4073. [CrossRef]
19. Waris, M.I.; Younas, A.; Ameen, A.; Rasool, F.; Wang, M.-Q. Expression Profiles and Biochemical Analysis of Chemosensory Protein 3 from Nilaparvata Lugens (Hemiptera: Delphacidae). *J. Chem. Ecol.* **2020**, *46*, 363–377. [CrossRef]
20. Zhou, X.-H.; Ban, L.-P.; Iovinella, I.; Zhao, L.-J.; Gao, Q.; Felicioli, A.; Sagona, S.; Pieraccini, G.; Pelosi, P.; Zhang, L.; et al. Diversity, Abundance, and Sex-Specific Expression of Chemosensory Proteins in the Reproductive Organs of the Locust Locusta Migratoria Manilensis. *Biol. Chem.* **2013**, *394*, 43–54. [CrossRef]
21. Maleszka, J.; Forêt, S.; Saint, R.B.; Maleszka, R. RNAi-Induced Phenotypes Suggest a Novel Role for a Chemosensory Protein CSP5 in the Development of Embryonic Integument in the Honeybee (Apis Mellifera). *Dev. Genes Evol.* **2007**, *217*, 189–196. [CrossRef]
22. Nomura, A.; Kawasaki, K.; Kubo, T.; Natori, S. Purification and Localization of P10, a Novel Protein That Increases in Nymphal Regenerating Legs of Periplaneta Americana (American Cockroach). *Int. J. Dev. Biol.* **1992**, *36*, 391–398. [PubMed]
23. Forêt, S.; Wanner, K.W.; Maleszka, R. Chemosensory Proteins in the Honey Bee: Insights from the Annotated Genome, Comparative Analyses and Expressional Profiling. *Insect Biochem. Mol. Biol.* **2007**, *37*, 19–28. [CrossRef] [PubMed]
24. Zhu, J.; Iovinella, I.; Dani, F.R.; Liu, Y.-L.; Huang, L.-Q.; Liu, Y.; Wang, C.-Z.; Pelosi, P.; Wang, G. Conserved Chemosensory Proteins in the Proboscis and Eyes of Lepidoptera. *Int. J. Biol. Sci.* **2016**, *12*, 1394–1404. [CrossRef] [PubMed]
25. Dani, F.R.; Michelucci, E.; Francese, S.; Mastrobuoni, G.; Cappellozza, S.; La Marca, G.; Niccolini, A.; Felicioli, A.; Moneti, G.; Pelosi, P. Odorant-Binding Proteins and Chemosensory Proteins in Pheromone Detection and Release in the Silkmoth Bombyx Mori. *Chem. Senses* **2011**, *36*, 335–344. [CrossRef] [PubMed]
26. Iovinella, I.; Dani, F.R.; Niccolini, A.; Sagona, S.; Michelucci, E.; Gazzano, A.; Turillazzi, S.; Felicioli, A.; Pelosi, P. Differential Expression of Odorant-Binding Proteins in the Mandibular Glands of the Honey Bee According to Caste and Age. *J. Proteome Res.* **2011**, *10*, 3439–3449. [CrossRef]
27. Jacquin-Joly, E. Functional and Expression Pattern Analysis of Chemosensory Proteins Expressed in Antennae and Pheromonal Gland of Mamestra Brassicae. *Chem. Senses* **2001**, *26*, 833–844. [CrossRef]
28. Schiff, N.; Goulet, H.; Smith, D.; Boudreault, C.; Wilson, A.; Scheffler, B.E. Siricidae (Hymenoptera: Symphyta: Siricoidea) of the Western Hemisphere. *Can. J. Arthropod Identif.* **2012**, *21*, 1–305. [CrossRef]
29. Wang, M.; Wang, L.; Fu, N.; Gao, C.; Ao, T.; Ren, L.; Luo, Y. Comparison of Wing, Ovipositor, and Cornus Morphologies between Sirex Noctilio and Sirex Nitobei Using Geometric Morphometrics. *Insects* **2020**, *11*, 84. [CrossRef]
30. Fukuda, H.; Hijii, N. Different Parasitism Patterns of Two Hymenopterous Parasitoids (Ichineumonidae and Ibaliidae) Depending on the Development of Sirex Nitobei (Hym., Siricidae). *J. Appl. Entomol.* **1996**, *120*, 301–305. [CrossRef]
31. Kobayashi, T.; Sasaki, K.; Enda, N. Correlation between Sirex Nitobei and Amylostereum Areolatum, Associated with the Death of Japanese Pine Trees during Winter Season. *J. Jpn. For. Soc.* **1978**, *60*, 405–411.
32. Fitza, K.N.E.; Tabata, M.; Kanzaki, N.; Kimura, K.; Garnas, J.; Slippers, B. Host Specificity and Diversity of Amylostereum Associated with Japanese Siricids. *Fungal Ecol.* **2016**, *24*, 76–81. [CrossRef]
33. Xiao, G.R.; Huang, X.Y.; Zhou, S.Z.; Wu, J.; Zhang, P. *Economic Sawfly Fauna of China*; Tianze Eldonejo: Beijing, China, 1991; pp. 37–42.
34. Guo, B.; Hao, E.; Qiao, H.; Wang, J.; Wu, W.; Zhou, J.; Lu, P. Antennal Transcriptome Analysis of Olfactory Genes and Characterizations of Odorant Binding Proteins in Two Woodwasps, Sirex Noctilio and Sirex Nitobei (Hymenoptera: Siricidae). *BMC Genom.* **2021**, *22*, 172. [CrossRef] [PubMed]
35. Livak, K.J.; Schmittgen, T.D. Analysis of Relative Gene Expression Data Using Real-Time Quantitative PCR and the 2(-Delta Delta C(T)) Method. *Methods* **2001**, *25*, 402–408. [CrossRef] [PubMed]
36. Bordoli, L.; Kiefer, F.; Arnold, K.; Benkert, P.; Battey, J.; Schwede, T. Protein Structure Homology Modeling Using SWISS-MODEL Workspace. *Nat. Protoc.* **2009**, *4*, 1–13. [CrossRef]
37. Luthy, R.; Bowie, J.U.; Eisenberg, D. Assessment of Protein Models with Three-Dimensional Profiles. *Nature* **1992**, *356*, 83–85. [CrossRef]
38. Colovos, C.; Yeates, T.O. Verification of Protein Structures: Patterns of Nonbonded Atomic Interactions. *Protein Sci.* **1993**, *2*, 1511–1519. [CrossRef]
39. Laskowski, R.A.; Moss, D.S.; Thornton, J.M. Main-Chain Bond Lengths and Bond Angles in Protein Structures. *J. Mol. Biol.* **1993**, *231*, 1049–1067. [CrossRef]
40. Abraham, M.J.; Murtola, T.; Schulz, R.; Páll, S.; Smith, J.C.; Hess, B.; Lindahl, E. GROMACS: High Performance Molecular Simulations through Multi-Level Parallelism from Laptops to Supercomputers. *SoftwareX* **2015**, *1–2*, 19–25. [CrossRef]
41. Ren, J.; Yuan, X.; Li, J.; Lin, S.; Yang, B.; Chen, C.; Zhao, J.; Zheng, W.; Liao, H.; Yang, Z.; et al. Assessing the Performance of the G_mmpbsa Tools to Simulate the Inhibition of Oseltamivir to Influenza Virus Neuraminidase by Molecular Mechanics Poisson–Boltzmann Surface Area Methods. *J. Chin. Chem. Soc.* **2020**, *67*, 46–53. [CrossRef]
42. Wang, J.; Wolf, R.M.; Caldwell, J.W.; Kollman, P.A.; Case, D.A. Development and Testing of a General Amber Force Field. *J. Comput. Chem.* **2004**, *25*, 1157–1174. [CrossRef]

43. Sousa da Silva, A.W.; Vranken, W.F. ACPYPE-AnteChamber PYthon Parser InterfacE. *BMC Res. Notes* **2012**, *5*, 367. [CrossRef] [PubMed]
44. Awasthi, M.; Jaiswal, N.; Singh, S.; Pandey, V.P.; Dwivedi, U.N. Molecular Docking and Dynamics Simulation Analyses Unraveling the Differential Enzymatic Catalysis by Plant and Fungal Laccases with Respect to Lignin Biosynthesis and Degradation. *J. Biomol. Struct. Dyn.* **2015**, *33*, 1835–1849. [CrossRef] [PubMed]
45. Calvello, M.; Guerra, N.; Brandazza, A.; D'Ambrosio, C.; Scaloni, A.; Dani, F.R.; Turillazzi, S.; Pelosi, P. Soluble Proteins of Chemical Communication in the Social Wasp Polistes Dominulus. *Cell. Mol. Life Sci. (CMLS)* **2003**, *60*, 1933–1943. [CrossRef] [PubMed]
46. Ishida, Y.; Chiang, V.; Leal, W.S. Protein That Makes Sense in the Argentine Ant. *Naturwissenschaften* **2002**, *89*, 505–507. [CrossRef]
47. González, D.; Zhao, Q.; McMahan, C.; Velasquez, D.; Haskins, W.E.; Sponsel, V.; Cassill, A.; Renthal, R. The Major Antennal Chemosensory Protein of Red Imported Fire Ant Workers. *Insect Mol. Biol.* **2009**, *18*, 395–404. [CrossRef]
48. Zhao, Y.; Wang, F.; Zhang, X.; Zhang, S.; Guo, S.; Zhu, G.; Liu, Q.; Li, M. Transcriptome and Expression Patterns of Chemosensory Genes in Antennae of the Parasitoid Wasp Chouioia Cunea. *PLoS ONE* **2016**, *11*, e0148159. [CrossRef]
49. Peng, Y.; Wang, S.-N.; Li, K.-M.; Liu, J.-T.; Zheng, Y.; Shan, S.; Yang, Y.-Q.; Li, R.-J.; Zhang, Y.-J.; Guo, Y.-Y. Identification of Odorant Binding Proteins and Chemosensory Proteins in Microplitis Mediator as Well as Functional Characterization of Chemosensory Protein 3. *PLoS ONE* **2017**, *12*, e0180775. [CrossRef]
50. Tomaselli, S.; Crescenzi, O.; Sanfelice, D.; Ab, E.; Wechselberger, R.; Angeli, S.; Scaloni, A.; Boelens, R.; Tancredi, T.; Pelosi, P.; et al. Solution Structure of a Chemosensory Protein from the Desert Locust Schistocerca Gregaria. *Biochemistry* **2006**, *45*, 10606–10613. [CrossRef]
51. Campanacci, V.; Lartigue, A.; Hällberg, B.M.; Jones, T.A.; Giudici-Orticoni, M.-T.; Tegoni, M.; Cambillau, C. Moth Chemosensory Protein Exhibits Drastic Conformational Changes and Cooperativity on Ligand Binding. *Proc. Natl. Acad. Sci. USA* **2003**, *100*, 5069–5074. [CrossRef]
52. Li, Y.-N.; Hao, E.-H.; Li, H.; Yuan, X.-H.; Lu, P.-F.; Qiao, H.-L. Computational Interaction Analysis of Sirex Noctilio Odorant-Binding Protein (SnocOBP7) Combined with Female Sex Pheromones and Symbiotic Fungal Volatiles. *Agronomy* **2021**, *11*, 2461. [CrossRef]
53. Fan, J. *cDNA Isolation and Protein Expression of OBP3 in Six Insects and Identification of Proteins Associated with Olfaction in Sitobion Avenae*; Chinese Academy of Agricultural Sciences: Beijing, China, 2011.
54. Tian, Z.; Liu, J.; Zhang, Y. Structural Insights into Cydia Pomonella Pheromone Binding Protein 2 Mediated Prediction of Potentially Active Semiochemicals. *Sci. Rep.* **2016**, *6*, 22336. [CrossRef] [PubMed]
55. Venthur, H.; Machuca, J.; Godoy, R.; Palma-Millanao, R.; Zhou, J.; Larama, G.; Bardehle, L.; Quiroz, A.; Ceballos, R.; Mutis, A. Structural Investigation of Selective Binding Dynamics for the Pheromone-binding Protein 1 of the Grapevine Moth, Lobesia Botrana. *Arch. Insect Biochem. Physiol* **2019**, *101*, e21557. [CrossRef] [PubMed]
56. Du, W.; Jiao, J.; Wang, Q. Brief report on luring and collecting Sirex nitobei by trap log. *Heilongjiang Agric. Sci.* **2011**, *5*, 57–59.
57. Bao, M.; Qiao, H.; Shi, J.; Luo, Y.; Lu, P. Research progress in reproductive behavior and chemical ecological regulation of the european woodwasp (Sirex noctilio), a severe invasive pest. *Sci. Silvae Sin.* **2020**, *56*, 127–141. [CrossRef]
58. Xu, Q.; Sun, X.-T.; Lu, P.-F.; Luo, Y.-Q.; Shi, J. Volatile Profiles of Three Tree Species in the Northeastern China and Associated Effects on Sirex Noctilio Activity. *J. Plant Interact.* **2019**, *14*, 334–339. [CrossRef]
59. Wang, M.; Bao, M.; Ao, T.; Ren, L.; Luo, Y. Population Distribution Patterns and Ecological Niches of Two Sirex Species Damaging Pinus Sylvestris Var. *Mongolica. Chin. J. Appl. Entomol.* **2017**, *54*, 924–932.
60. Boroczky, K.; Crook, D.J.; Francese, J.A.; Mastro, V.C.; Tumlinson, J.H. Chemical Ecology of Sirex Noctilio. In *Proceedings 19th U.S. Department of Agriculture Interagency Research Forum on Invasive Species 2008*; McManus, K.A., Gottschalk, K.W., Eds.; 2009.
61. Bashford, R. The Development of Static Trapping Systems to Monitor for Wood-Boring Insects in Forestry Plantations. *Aust. For.* **2008**, *71*, 236–241. [CrossRef]
62. Li, D.; Shi, J.; Lu, M.; Ren, L.; Zhen, C.; Luo, Y. Detection and Identification of the Invasive Sirex Noctilio (Hymenoptera: Siricidae) Fungal Symbiont, Amylostereum Areolatum (Russulales: Amylostereacea), in China and the Stimulating Effect of Insect Venom on Laccase Production by A. *Areolatum YQL03. J. Econ. Entomol.* **2015**, *108*, 1136–1147. [CrossRef]
63. Li, Z.; Liu, L.; Zong, S.; Tao, J. Molecular Characterization and Expression Profiling of Chemosensory Proteins in Male Eogystia Hippophaecolus (Lepidoptera: Cossidae). *J. Entomol. Sci.* **2021**, *56*, 217–234. [CrossRef]
64. Nagnan-Le Meillour, P. Chemosensory Proteins from the Proboscis of Mamestra Brassicae. *Chem. Senses* **2000**, *25*, 541–553. [CrossRef]
65. Thompson, B.M.; Grebenok, R.J.; Behmer, S.T.; Gruner, D.S. Microbial Symbionts Shape the Sterol Profile of the Xylem-Feeding Woodwasp, Sirex Noctilio. *J. Chem. Ecol.* **2013**, *39*, 129–139. [CrossRef] [PubMed]
66. Thompson, B.M.; Bodart, J.; McEwen, C.; Gruner, D.S. Adaptations for Symbiont-Mediated External Digestion in Sirex Noctilio (Hymenoptera: Siricidae). *Ann. Entomol. Soc. Am.* **2014**, *107*, 453–460. [CrossRef]
67. Buchanan, P.K. Aphyllophorales in Australasia. *Aust. Systematic Bot.* **2001**, *14*, 417. [CrossRef]
68. Wang, Y.; Shi, T.-F.; Qi, L.; Liu, F.; Zhu, Y.-J.; Hou, C.; Yu, L.-S. Spatiotemporal expression levels of three chemosensory proteins in adult Apis mellifera ligustica workers. *Chin. J. Appl. Entomol.* **2018**, *55*, 71–78.